Elaboration, Characterization Of $LaOHCO_3$, $La_2O_2CO_3$ And La_2O_3 Phases And Their Gas Solid Interactions With CH_4 And CO Gases

Bahcine Bakiz[a,b], Frédéric Guinneton[a], Madjid Arab[a], Abdeljalil Benlhachemi[b], Jean-Raymond Gavarria[1]

(a) Institut Matériaux Microélectronique & Nanosciences de Provence, UMR CNRS 6242, Université du SUD Toulon-Var, BP 20132, 83957 La Garde, Cedex, France
(b) Laboratoire Matériaux et Environnement, Faculté des Sciences, Université Ibn Zohr, B.P 8106, 80000, Agadir, Morocco

Abstract: The aim of this study was to compare the reactivity of three lanthanum-based phases in presence of methane CH_4 or carbon monoxide CO gases. The hydroxycarbonate $LaOHCO_3$ was synthesized from a new specific precipitation route. From this hydroxycarbonate phase, the dioxycarbonate $La_2O_2CO_3$ and the oxide La_2O_3 were prepared by thermal decomposition process. The polycrystalline samples were characterized by X-ray diffraction, scanning (SEM) and transmission (TEM) electron microscopy. Statistical analyses of grain sizes and morphologies were carried out from TEM analyses. The three samples were then subjected to interactions with air-CH_4 and air-CO flows, at various temperatures. The oxidation of CH_4 and CO into CO_2 interacting with the samples was studied using Fourier Transform infrared spectroscopy. Finally, the reactivity of samples is discussed.

Key words: lanthanum hydroxycarbonate, lanthanum dioxycarbonate, lanthanum oxide, elaboration, microstructural analyses, infrared spectroscopy, gas solid interactions.

[1] To whom correspondence must be addressed: e-mail: gavarri.jr@univ-tln.fr

I. Introduction

The general aim of this study was to investigate the potential application of ceramics phases in gas sensors or CO_2 absorbing devices for CO_2 capture. The lanthanum based system La_2O_3-CO_2-H_2O might be an interesting candidate for such applications, because the refractory ceramics phase La_2O_3 is sensitive to several types of gases: methane, carbon monoxide, H_2O and CO_2 molecules present in the surrounding atmosphere. At low temperature, the hydroxycarbonate $LaOHCO_3$ (denoted LHC) [1, 2] or dioxycarbonate $La_2O_2CO_3$ (denoted LOC) [3-6] could interact with water and CO_2, while at high temperature, the oxide La_2O_3 (L) [7-12] could only interact with the specific gas to be detected (like CH_4 or CO). This lanthanum-based La_2O_3-CO_2-H_2O system could attract a great deal of interest because lanthanum oxide is highly water absorbent and fast carbonation occurs in environments where CO_2 and H_2O are both present [13-15]. In this work, we mainly try to characterize the time- and temperature-dependence of these three L, LOC and LHC phases interacting with air-methane or air-carbon monoxide mixtures. One possible objective is to use the various temperature ranges at which each phase (LHC, LOC, or L) must be stable in the presence of H_2O vapor and/or CO_2 gas so that it can be used as sensitive phase interacting with an additional gas (e.g. methane CH_4 or carbon monoxide CO). For example, at sufficiently low temperatures, the LHC phase would be sensitive to water vapor; at intermediate temperatures, the LOC phase would be sensitive to CO_2 gas; and finally at higher temperatures the L phase would be insensitive to water or CO_2 and could only interact with CO or CH_4.

II. Experimental Details

II-1. Sample preparation

An original precipitation route, initially applied by us to cerium monoxycarbonate elaboration [16], allowed preparing the lanthanum hydroxycarbonate phase. A similar approach was proposed by Qing Li et al. [17] to obtain the cerium based phase $CeOHCO_3$.

The first step involved mixing three aqueous solutions: (1) $La(NO_3)_3 \cdot 6H_2O$, (2) urea $CO(NH_2)_2$ and (3) polyvinyl - pyrrolidone (PVP) polymer. The initial pH was 3.2. . In the second step, the solution was heated at 80°C in a reactor equipped with a vapor condenser. In all experiments, solutions were permanently agitated by means of a rotating magnet at a fixed rate of 300 rpm. During heating, the temperature was fixed, and the vapors were condensed

in a water-cooled circuit to prevent evaporation of the aqueous solution. A white solid precipitated. Figure 1 shows the various elaboration steps.

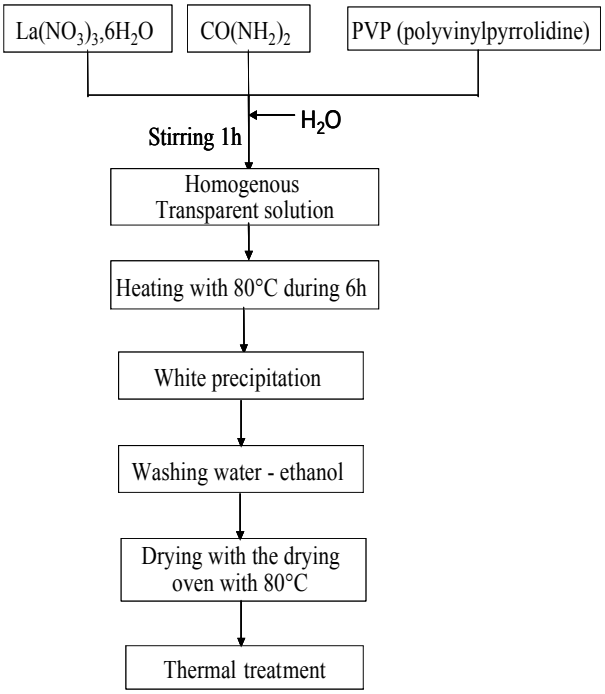

Fig.1: Chart for lanthanum hydroxycarbonate syntheses by precipitation, in presence of urea $CO(NH_2)_2$

II-2. Thermal analyses

The phase stabilities were determined as a function of the temperature by differential thermal analysis coupled with thermogravimetry (DTA-TG) using a SETARAM TG-DTA92 analyzer.

The resulting hydrated lanthanum hydroxycarbonate powder (95.1 mg) was placed in the analysis cell and heated with a linear temperature gradient from 25°C to 1100°C at a rate of 10°C per minute. Figure 2 reports the DTA-TG results. There are a series of decomposition steps with successive inflexion points at 180°C, 310°C, and a stability domain between 530 and 780°C. Finally, the last stable oxide phase was obtained above 880°C.

The first mass loss is attributed to the loss of water:

$LaOHCO_3 \cdot x\ H_2O \rightarrow LaOHCO_3 + x\ H_2O$, where x=1 (1)

The second mass loss is attributed to the first decomposition step with loss of one H_2O and one CO_2 from 2 LHC molecules:

$2\ LaOHCO_3 \rightarrow La_2O_2CO_3 + H_2O + CO_2$ (2)

The last mass loss is attributed to the loss of a further CO_2 molecular and formation of La_2O_3 oxide:

$La_2O_2CO_3 \rightarrow La_2O_3 + CO_2$ (3)

Table 1 compares the experimental and calculated weight losses.

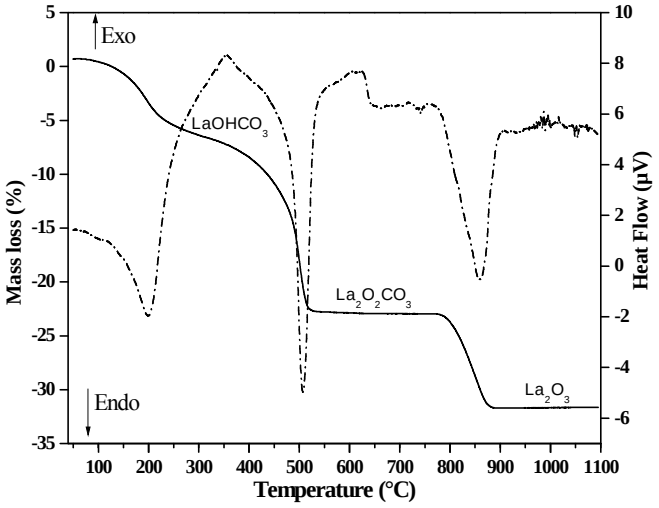

Fig.2: Thermal decomposition analysis (DTA-TG) of hydrated hydroxycarbonate: successive phases $LaOHCO_3$ (LHC), $La_2O_2CO_3$ (LOC), and La_2O_3 (L).

	Reactions from $2LaOHCO_3 \cdot H_2O$ to La_2O_3	Calculated weight loss (%)	Experimental weight loss (%)
Step 1	$2\ LaOHCO_3 \cdot H_2O \rightarrow 2\ LaOHCO_3 + 2\ H_2O$	7.7	7.8
Step 2	$2\ LaOHCO_3 \rightarrow La_2O_2CO_3 + H_2O + CO_2$	13.3	13.5
Step 3	$La_2O_2CO_3 \rightarrow La_2O_3 + CO_2$	11.9	11.7

Table1. Comparison of the experimental and calculated weight losses for $LaOHCO_3 \cdot H_2O$

II-3. Characterizations

II-3-1. X-ray diffraction:

X-ray diffraction patterns were recorded on a Siemens-Brucker D5000 diffractometer working in a θ–2θ mode, with a copper X-ray source (λ(Kα1) =1.5406 Å), Soller slides, and secondary monochromator.

Figure 3 (a-d) shows the X-ray diffraction patterns of:

- the LHC phase obtained after heating the solid precursor at 200°C (Fig. 3a),
- the tetragonal and hexagonal phases of LOC, obtained after heating the precursor at 500°C (Fig. 3b),
- the hexagonal phase of LOC (2), obtained at 620°C (Fig. 3c),
- the hexagonal phase of La_2O_3, obtained at 750°C (Fig. 3d).

The cell parameters were refined by means of the PARAM software from [18].

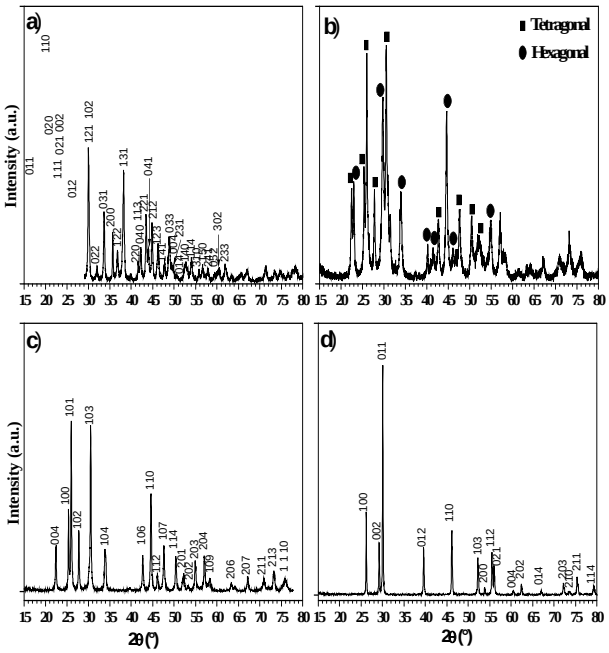

Fig.3: X-ray diffraction patterns of: a) $LaOHCO_3$ (LHC) at 200°C, b) $La_2O_2CO_3$ (LOC) at 500°C (tetragonal and hexagonal phases), c) $La_2O_2CO_3$ (hexagonal phase) at 620°C, and d) La_2O_3 at 750°C.

Phase/ composition	Cell parameters (Å)	Space group	Literature values (Å)
$LaOHCO_3$ at 200°C	a=5.042±0.007 b=8.574±0.009 c=7.391±0.008	Pmcn	a=5.033 b=8.598 c=7.401 [19]
$La_2O_2CO_3$ at 500°C	a=4.059±0.004 c=13.499±0.006	I4/mmm	a=4.063 c=13.500 JCPDS 25-0422
$La_2O_2CO_3$ at 620°C	a =4.076±0.002 c=15.964±0.007	$P6_3/mmc$	a=4.075 c=15.957 JCPDS 84-1963
La_2O_3 at 750°C	a =3.938± 0.001 c =6.127± 0.002	P321	a=3.937 c=6.129 [20]

Table 2: X-ray diffraction data: refined cell parameters of lanthanum-based hydroxycarbonate (LHC), dioxycarbonate (LOC), and oxide (L).

II-3-2. Microstructural analyses: Scanning and Transmission electron microscopy.

Preliminary images were obtained with a Philips XL30 scanning electron microscope (SEM) using a maximum voltage of 20 kV. Transmission electron microscopy (TEM) analyses were carried out using a Tecnai G2 microscope with a LaB6 source, operating at 200 kV.

Figure 4 shows an SEM image of hydroxycarbonate powder containing acicular agglomerates with sizes ranging between 3 to 5 µm. The transmission electron analysis in Figure 5 shows individual needles that resemble spindles with lengths of about 5 µm. The spindle in Figure 5b has two circles designating the two zones on which electron diffraction was performed. The two associated diffraction images of Figure 5c and 5d are similar and they show that one spindle is a pseudo-single crystal with a unique crystalline orientation.

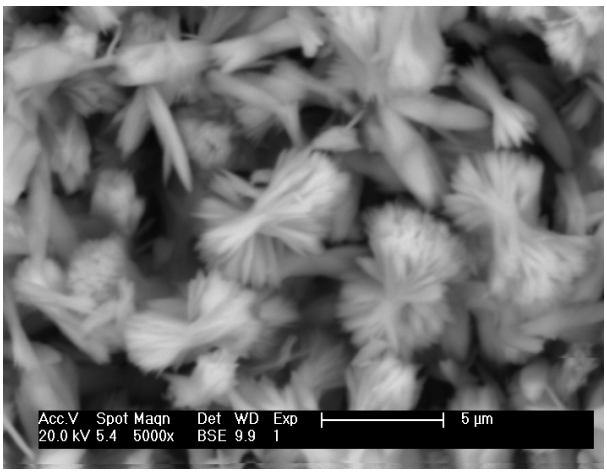

Fig.4: SEM image of lanthanum hydroxycarbonate (LHC) showing the presence of needles with lengths ranging between 2 and 5 µm.

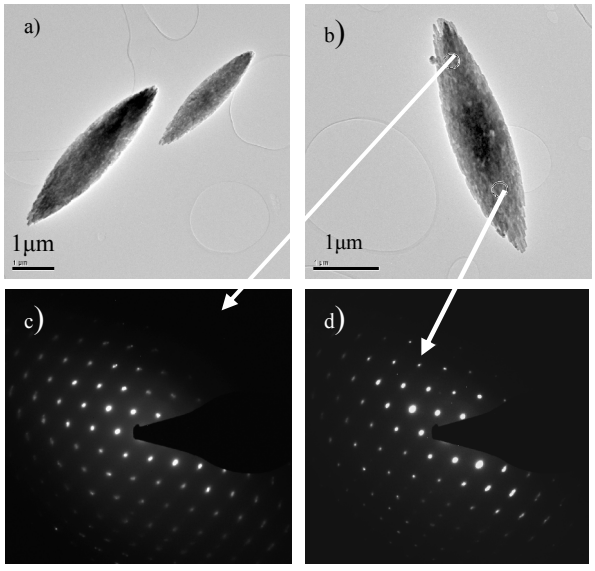

Fig.5: a) TEM images of LHC spindles; b) isolated LHC spindle: electron diffraction was performed on the two zones indicated by the two circles; c) and d) TEM electron diffraction of the two LHC spindle zones. The two similar diffraction images indicate that the spindles are pseudo-single crystals with a unique crystalline orientation.

The TEM image of Figure 6 shows that dioxycarbonate (LOC) grains, obtained from thermal

decomposition of LHC powder, have smaller dimensions (lengths of about 100 to 200 nm) with irregular rectangular shapes and that each grain is a pseudo-single crystal.

The TEM image of La_2O_3 oxide powder obtained from the thermal decomposition of the initial LHC powder shows the presence of small crystals having more regular morphologies, with main dimensions of 150 nm x 150 nm x 250 nm.

The three samples present three types of morphologies and grain sizes. If we assume that each grain is isolated, with the absence of closed agglomerates, the idealized specific surfaces of the L and LOC samples are smaller than the specific surface of the LHC sample. This might play an important role in the catalytic properties. We have performed a statistical analysis of grain sizes using image analyses for each sample and average dimensions were defined. From these analyses, the theoretical specific surfaces Rss = S/V were calculated.

The shape of the LHC grains has been assimilated to an ellipsoid with two a- and b-axis dimensions. The resulting volume is $V = 4/3\ (\pi\ a\ b^2)$ where a and b are average values of dimensions, and the surface area is: $S = 2\ \pi\ b\ (b+a)\ (\arcsin[e]/e)$, where

$e = \sqrt{(1-(b^2/a^2)}$.

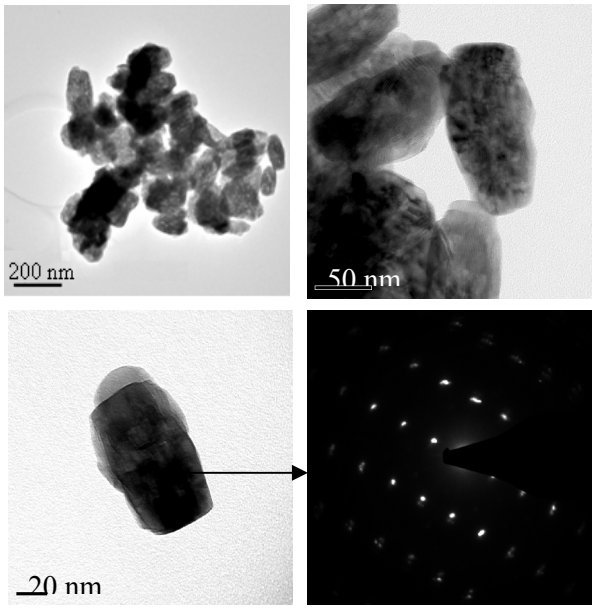

Fig.6: TEM images of LOC grains: pseudo-rectangular shapes, electron diffraction image of a pseudo-single crystal (hexagonal symmetry).

In the case of the LOC and L grains, a cubic form has been chosen to represent one average grain (average dimension a, volume: $V = a^3$, surface area: $S= 6a^2$). From these approximations, we have defined the idealized specific surface ratios Rss = S/V for each sample. The values for LHC, LOC, and L grains are: Rss(LHC) = 252 µm-1 (a = 2 µm and b = 0.45 µm), Rss(LOC) = 60 µm-1 (a = 0.1 µm), and Rss(L) = S/V = 40 µm-1 (a = 0.15 µm).

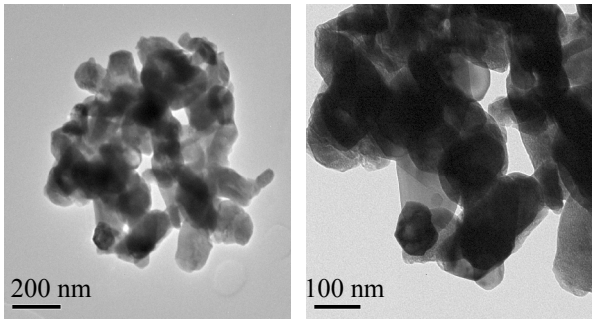

Fig.7: TEM images of lanthanum oxide obtained from the decomposition of LHC.

III. Solid-Gas Interactions

III-1. Reaction conversion device.

The polycrystalline samples (L, LCO, and LHC) were exposed to air-CH_4 and air-CO gas flows in a specific homemade heated cell. The various gas flows pass through each sample disposed in a cylindrical tube as a polycrystalline catalytic wall, heated at a fixed temperature. The emerging gases are then analyzed by Fourier transform infrared (FTIR) spectroscopy, using a FTIR Unicam-Mattson spectrometer working with cube corner technology. The FTIR equipment is used to determine the resulting amount of CO_2 after conversion of CH_4 or CO in the porous polycristalline wall. This homemade equipment has been described in a previous publication [21]. Figure 8 shows the experimental setup. The reactor is a cylindrical cell in which the sample can be exposed to reactive air-gas flows. The sample temperature is controlled by a thermocouple and stabilized at a given Treact value. A fixed mass (m_0=0.1 g for each test) of powder is placed between two porous (ZrO_2) separators. Blank experiments with these separators were systematically carried out to confirm the absence of activity in the cell itself. The gas flows, controlled by flowmeters (2500 ppm CO in air or CH_4 in air), passed through separator 1, then the sample, and finally separator 2, with a fixed slow speed (10 sccm). The reactor is placed in a furnace and heated at temperatures ranging between 150 °C and 525°C.

The reaction conversion effect is revealed by the appearance of the infrared absorption band of CO_2. The intensity of the CO_2 vibrational band, noted as $I(CO_2)$, is assumed to represent the capacity of the solid to convert CH_4 or CO into CO_2. The conversion

efficiency of the three polycrystalline samples was defined as being proportional to the intensities of the FTIR CO_2 vibrational bands (doublet at 2340 - 2360 cm-1), resulting from the overall reactions (4) and (4'):

$$CH_4 + 2\,O_2 \rightarrow CO_2 + 2H_2O \qquad (4)$$

$$CO + 1/2O_2 \rightarrow CO_2 \qquad (4')$$

To compare the conversion efficiencies of the L, LHC and LOC phases, it has been necessary to apply a specific experimental protocol that permits the analysis of the sole gases produced during a solid-gas reaction and avoids any environmental gas perturbations. This protocol is essential to differentiate between residual traces of environmental CO_2 and the CO_2 molecules produced during the solid-gas reaction.

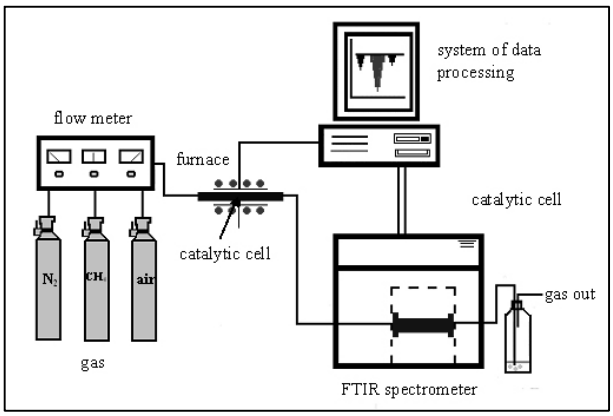

Fig.8: Homemade reactor (gas feed, furnace, FTIR analysis).

Each vibrational spectrum was recorded over a period of 10 s with intervals of 30 s between two spectra. The total exposure time to the catalyst was two hours. The conversion was analyzed at various fixed temperatures between 175°C to 525 °C. The conversion intensity was determined from measurements of the intensities of CO2 absorption bands, at a certain time t of the gas/solid interaction: in fact, these intensities were determined for a given FTIR measuring time during which a permanent flow of gas passed through the sample. The FTIR intensities of CH_4 or CO absorption peaks varied linearly with the air-gas composition. The value of $I(CO_2)$, expressed in arbitrary units (a.u.), is directly linked to the derivative dX/dt of the total amount of CO_2 (X) formed during the conversion reaction and also depends on time t. In other words, the integral of the dX/dt curve should directly deliver the total amount of CO_2 associated with CH_4 or CO conversion by the system.

III-2. Results

All experimental data associated with conversion depend on the air/Gas composition, and on the specific surfaces of active powder samples.

The catalytic properties versus temperature of the powders for both gases (CH_4 and CO) have been evaluated under the same conditions. The results are shown in Figures 9 and 10. We observed the same behavior for both gases: the reactivities have significant values at two starting temperatures (425 °C for CH_4 and 175 °C for CO) and reach a maximum equilibrium level after about 20-25 min. These temperatures are required to obtain a significant conversion reaction of CH_4 and CO into CO_2. The maximum equilibrium levels increase with temperature and reach a limit of 525°C for CH_4 and 300°C for CO. Before these equilibrium states are reached, the kinetic reactions, expressed by the slope ($\Delta I / \Delta t$) obtained during the first 15 minutes, also change with temperature. This explains the increasing conversion speed as the temperature increases.

III-3-1. Interactions with methane.

Figure 9 (a-c) gives the experimental data (in arbitrary units or a.u.) of the conversion intensities $I(CO_2)$ of the two L and LOC phases interacting with air-CH4 flows. In Figure 9a, the interaction of CH4 with the L sample is characterized by a saturation level $I(CO_2)$max, which increases with catalysis temperature. The plateau is reached after about 20 minutes.

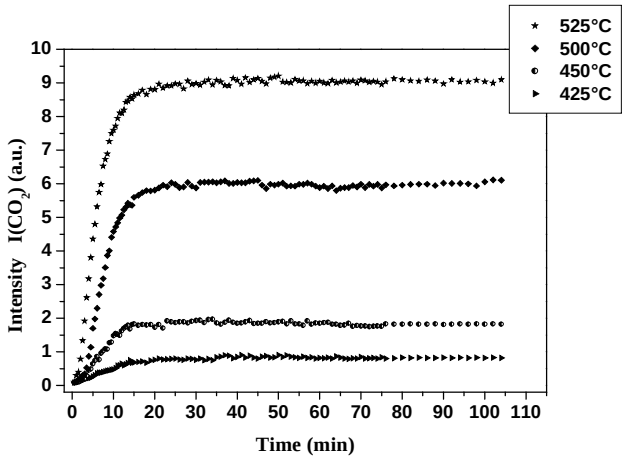

Fig.9a: La_2O_3/CH_4 interaction. FTIR intensity $I(CO_2)$ associated with the conversion of CH_4 interacting with La_2O_3 as a function of time at fixed temperatures (absolute surface $I(CO_2)$ of vibration band in arbitrary units).

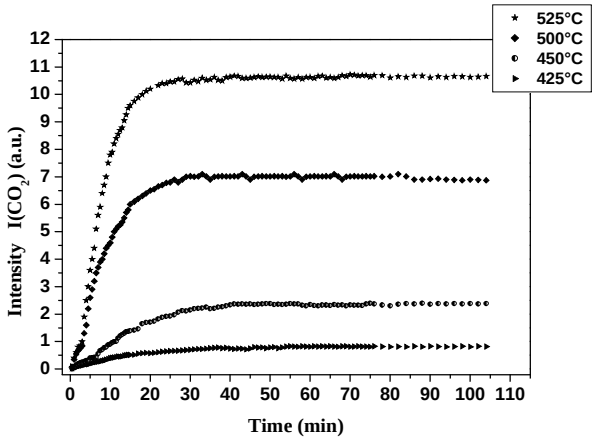

Fig.9b: LOC/CH_4 interactions. FTIR intensity I(CO_2) associated with the conversion of CH_4 interacting with $La_2O_2CO_3$ as a function of time and temperature (absolute surface of vibration band in arbitrary units).

III-3-2. Interactions with carbon monoxide.

Figure 10 (a-c) gives the experimental data of the conversion intensities I(CO_2) of each L, LHC, and LOC phases interacting with air-CO flows (2500 ppm CO in air). To allow comparisons between the individual intensities I(CO_2) of the LHC, LOC, and L phases, we calculated the effective exposed surface areas for each solid catalyst taking into account the mass introduced into the reactor cell. The effective volume of solids (Vi with index i for LHC, LOC, or L) exposed to gases can be calculated from the densities (μ_i) of the LHC, LOC, or L phases: $V_i = m_0/\mu_i$. The exposed surface areas Si of each catalyst can be evaluated from their theoretical specific surfaces Rss= S/V: $S_i = Rss.V_i$. The exposed surface areas Si are used as scale factors in our determination of the normalized intensities $I_i^* = I_i(CO2)/S_i$.

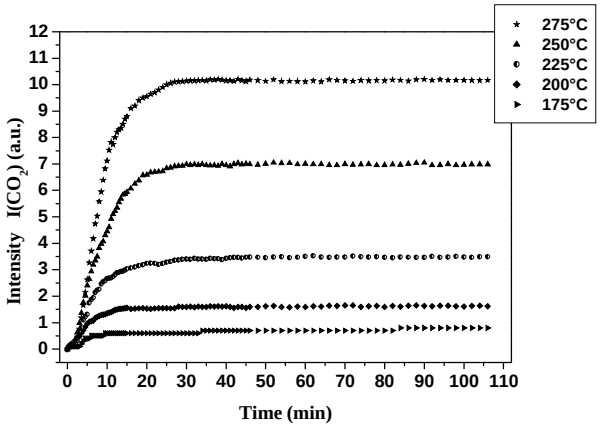

Fig.10a: CO/La_2O_3 interactions. FTIR intensity I(CO_2) associated with the conversion of CO interacting with La_2O_3 as a function of time and temperature (absolute surface of vibration band in arbitrary units).

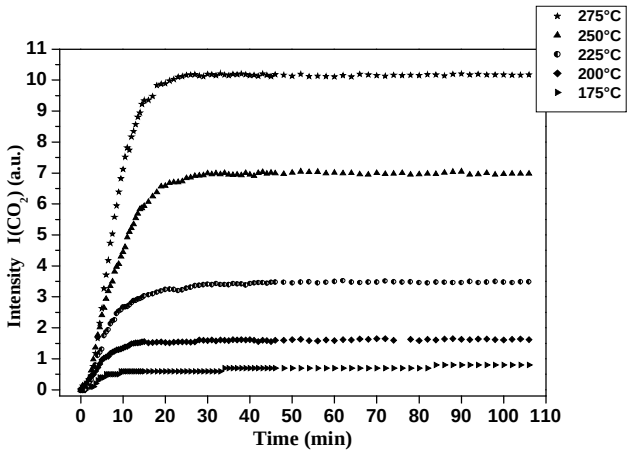

Fig.10b: CO/LOC interactions. FTIR intensity I(CO_2) associated with the conversion of CO interacting with $La_2O_2CO_3$ as a function of time and temperature (absolute surface of vibration band in arbitrary units).

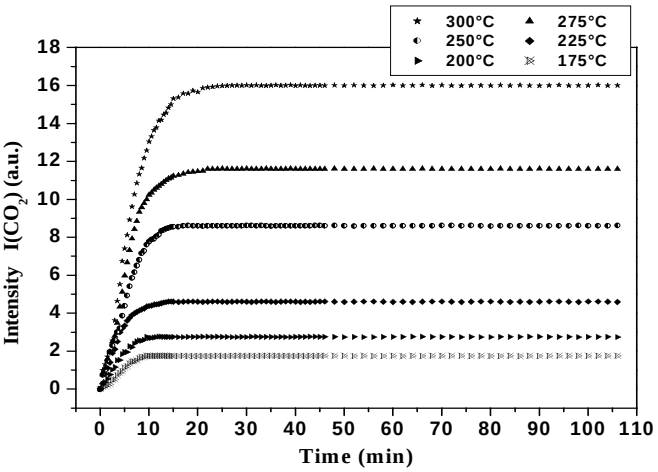

Fig.10c: CO/LHC interactions. FTIR intensity I(CO_2) associated with the conversion of CO interacting with $LaOHCO_3$ as a function of time and temperature (absolute surface of vibration band in arbitrary units).

Tables 3 and 4 give the normalized maximum conversion intensities $I_i^*(CO_2)$ that take account of the calculated ratios Rss=S/V and the calculated volumes V_i.

Table 3 compares the maximum conversion intensities of the L and LOC solids interacting with CH_4 air flows as a function of the temperature. The LOC and L phases show an increasing conversion intensity in the presence of air-CH_4 flows, with thermal activation in the temperature range between 425 and 525 °C. Let us recall that LHC does not significantly interact up to 350°C (for CH_4 in air) and that it decomposes above this temperature. Table 4 compares the maximum conversion intensities of the L, LOC, and LHC phases interacting with CO-air flows. The conversion intensity increases for the LHC, LOC, and L phases. The reactivity with CO is

observed at a relatively low temperature compared to the temperature range of CH4 activity. The LHC phase presents an interesting low (but significant) action on CO-air flows. We must point out that experiments at 275°C under air flow proved that the LHC phase was stable and did not deliver any CO_2 gas as a result of partial decomposition.

In Tables 3 and 4, we clearly observe that, for a given temperature, the conversion intensity $I_i*(CO_2)$ per surface unit is higher for La_2O_3 than for the LOC phase. In the case of CO conversion, for a given temperature, the $I_i*(CO_2)$ intensities are greater for La_2O_3 than for LOC and LHC phases. These differences in reactivities, expressed for surface units of samples, can be interpreted from the differences in natures of grain surfaces. The LHC phase is constituted of directly synthesized large grains having a needle like morphology. The LOC and L phases are obtained from a thermal decomposition process: grain sizes are smaller and grain morphology results from decomposition of initial LHC needles. The LOC phase results from a reorganization of CO_3^{2-} ions after elimination of one water molecule and one CO_2 molecule from the LHC lattice. The L structure results from the elimination of CO_2 molecules and the structural reorganization gives rise to small L particles with highly active surfaces. This enhanced activity is generally associated with the existence of surface defects and mobile oxygen atoms.

Sample Density g.cm^{-3}	R_{ss} = S/V (μm^{-1})	S_i=Rss* ($m_0/\mu i$) (m^2)	T (°C)	$I_i(CO_2)_{max}$	$I_i*(CO_2)$ = $I_i(CO_2)_{max}$/ S_i
$La_2O_2CO_3$ μ=2.60	60	2.307	425	0.82	0.35
			450	2.38	1.03
			500	6.88	2.98
			525	10.66	4.62
La_2O_3 μ=6.51	40	0.614	425	0.83	1.35
			450	0.82	1.34
			500	6.11	9.95
			525	9.02	14.70

Table 3: Normalized maximum CO_2 absorption band intensities $I_i*(CO_2)$ in the presence of air-CH_4 flows interacting with the solids LOC and L. No action for LHC sample.

Sample Density	R_{ss} =S/V (μm^{-1})	S_i=Rss* ($m_0/\mu i$) (m^2)	T (°C)	$I_i(CO_2)_{max}$	$I_i*(CO_2)$= $I_i(CO_2)_{max}$ S_i
$LaOHCO_3$ μ =4.48 g.cm^{-3}	252	5.625	175	1.75	0.31
			200	2.74	0.49
			250	8.62	1.53
			275	11.6	2.06
$La_2O_2CO_3$ μ=2.60 0g.cm^{-3}	60	2.307	175	0.8	0.35
			200	1.62	0.70
			250	6.98	3.02
			275	10.16	4.40
La_2O_3 μ=6.51 g.cm^{-3}	40	0.614	175	0.54	0.88
			200	0.71	1.15
			250	5.98	9.74
			275	7.4	12.05

Table 4: Normalized maximum CO_2 absorption band intensities $I_i*(CO_2)$ in the presence of air-CO flows interacting with the solids LHC, LOC, and L.

Finally, the large difference observed in the thermal range in which conversion occurs for CH4 and CO can be easily explained by the well-known stability of CH_4 associated with the complex steps of the catalytic decomposition in the case of this molecule.

IV. Conclusion

A new synthesis route of the lanthanum hydroxycarbonate has been proposed. This phase is stable up to 350°C. The thermal decomposition delivers the intermediate dioxycarbonate and oxide phases. The interest of these three phases resides in their different thermal stabilities and different gas solid interactions with CH_4 and CO. We have evidenced different behaviors of the three phases LHC, LOC and L in presence of CH_4-air and CO-air flows. The oxidation of CO occurs at low temperature for the three phases, while higher temperatures are required for the conversion of CH_4 into CO_2. Consequently, the $LaOHCO_3$ phase is not sensitive to CH_4 in its stability temperature range. It should be noted that the polycrystalline solids, LHC, LOC, and L, exhibit increasing reactivities in the presence of air-CO gases. Finally, the most interesting system for gas-sensor technologies should be the LHC phase: it might be sensitive to CO at low temperatures, but not sensitive to CH_4 in the same temperature range. As the temperature increases, the LHC could then decompose into the LOC and L phases. At high temperatures,

these last phases could be sensitive to CH_4 and CO. New studies are planned to correlate these behaviors with the electrical resistive properties and to evaluate the interest of such systems in gas-sensor technologies.

Acknowledgements. We gratefully acknowledge the Provence–Alpes–Côte d'Azur Regional Council, the General Council of Var, and the agglomeration community of Toulon Provence Mediterranean for their helpful financial supports. This work was developed in the general framework of ARCUS CERES project (2008-2010).

V. References

[1] H. Wakita and S. Kinoshita, "A synthetic study of the solid solutions in the systems and $La_2(CH_3)_3 \cdot 8H_2O$-$Ce_2(CO_3)_3 \cdot 8H_2O$and $La(OH)CO_3$-$Ce(OH)CO_3$"; Bulletin of the Chemical Society of Japan, 52 (1979) 428–432.

[2] O. K. Nikol'skaya and L. N. Dem'yanets, "Hydrothermal crystallization in the systems $La_2(CO_3)_3 \cdot 6H_2O$-$CaCO_3(BaCO_3)$-R-H_2O(R = Na_2, $CO_3K_2CO_3$, $NaHCO_3$, $KHCO_3$, NaCl, NH_4Cl, $CO(NH_2)_2$)"; Inorganic Materials, vol. 41, no. 11, pp. 1206–1212, 2005.

[3] M. L. Panchula and M. Akinc, "Morphology of lanthanum carbonate particles prepared by homogeneous precipitation"; Journal of the European Ceramic Society, 16 (1996) 833–841.

[4] S. Irusta, L.M. Cornaglia, E.A. Lombardo, "Effects of rhodium and platinum on the reactivity of lanthanum phases"; Materials Chemistry and Physics 86 (2004) 440–447.

[5] S. Valange, A. Beauchaud, J. Barrault, Z. Gabelica, M. Daturi, and F. Can, "Lanthanum oxides for the selective synthesis of phytosterol esters: correlation between catalytic and acid-base properties"; Journal of Catalysis, 251 (2007)113–122.

[6] A.N. Shirsat, M. Ali, K.N.G. Kaimal, S.R. Bharadwaj, D. Das, "Thermochemistry of $La_2O_2CO_3$ decomposition"; Thermochimica Acta 399 (2003) 167–170.

[7] Gamal A.M. Hussein, Hamdy M. Ismail, "Characterization of lanthanum oxide formed as a final decomposition product of lanthanum acetylacetonate: thermoanalytical, spectroscopic and microscopic studies"; Powder Technology 84 (1995) 185-190.

[8] A.E. Gobichon, J.P. Auffredic, D. Louer, "Thermal decomposition of neutral and basic lanthanum nitrates studied withtemperature-dependent powder diffraction and thermogravimetric analysis"; Solid State Ionics, 93 (1997) 51-64.

[9] B.A.A. Balboul, A.M. El-Roudi, S. Ebthal, A.G. Othman, "Non-isothermal studies of the decomposition course of lanthanum oxalate decahydrate"; Thermochim. Acta. 387 (2002) 109–114.

[10] P. Jeevanandam, Yu. Koltypin, O. Palchik and A. Gedanken, "Synthesis of morphologically controlled lanthanum carbonate particles using ultrasound irradiation"; J. Mater. Chem. 11 (2001) 869-873.

[11] B. Bakiz, K. Ouzaouit, A. Benlhachemi, A. Essoumhi, S.Villain, H. Benyaich and J.R. Gavarri, "Multiphase lanthanum hydroxycarbonates and langasite ceramics for gas sensors; Physical and Chemical News, 41 (2008) 55-60.

[12] K. Ouzaouit, B. Bakiz, S. Villain, A. Benlhachemi, A. Eessoumhi, H. Benyaich, F. Guinneton, J-R. Gavarri, "Lanthanum hydroxycarbonates and langasite ceramics: staility, infrared spectroscopy and electrical behaviors; Inzynieria Materialowa, NR 3-4 (2007) 330-333.

[13] T. Esaka, K. Motoike, "Absorption and desorption of carbon dioxide in the rare earth oxide-doped Bi_2O_3 powder"; J Alloy Compd. 408–412 (2006) 480–483.

[14] T. Esaka, K. Motoike; "CO_2 absorption and desorption of Bi_2O_3–La_2O_3 powders prepared by mechanical synthesis"; Mater. Res. Bull. 39 (2004) 1581–1587.

[15] Todd J. Toops, Arden B. Walters, M. Albert Vannice, "The effect of CO_2 and H_2O on the kinetics of NO reduction by CH_4 over a La_2O_3/γ -Al_2O_3 catalyst; J. Catal. 214 (2003) 292–307.

[16] B. Bakiz, F. Guinneton, J.P. Dallas, S. Villain, J.R. Gavarri, "From cerium oxycarbonate to nanostructured ceria: relations between synthesis, thermal process and morphologies"; J. Cryst. Growth. 310 (2008) 3055-3061.

[17] Qing Li, H. Zhaohui, S. Mingwang, L. Xianming, Q. Yitai, "Preparation of cerium hydroxycarbonate by a surfactant-assisted route"; J. Phys. Chem. Solids 64 (2003) 295.

[18] J.F.Berar, Ecole Centrale de Paris, 92295 Châtenay – Malabry (1989) Private Communication.

[19] Z. Han, Q. Yang, G.Q. Luc, "Crystalline lanthanum hydroxycarbonates with controlled phases and varied morphologies prepared on non-crystalline substrates"; J Solid State Chem 177 (2004) 3709–3714.

[20] R. Vali and S.M. Hosseini, "First-principles study of structural, dynamical, and dielectric properties of A-La_2O_3"; Comp Mater Sci 31 (2004) 125–130.

[21] P. Nowakowski, S. Villain, A. Kopia, I. Suliga, J.R. Gavarri, "Catalytic conversion of air–methane flow by nanostructured ruthenium dioxide: FTIR spectroscopy and modeling; Appl Surf Sci 254 (2008) 5675–5682